On the Way to *trans*-Coordinating Tridentate Pyrazolylborate Ligands

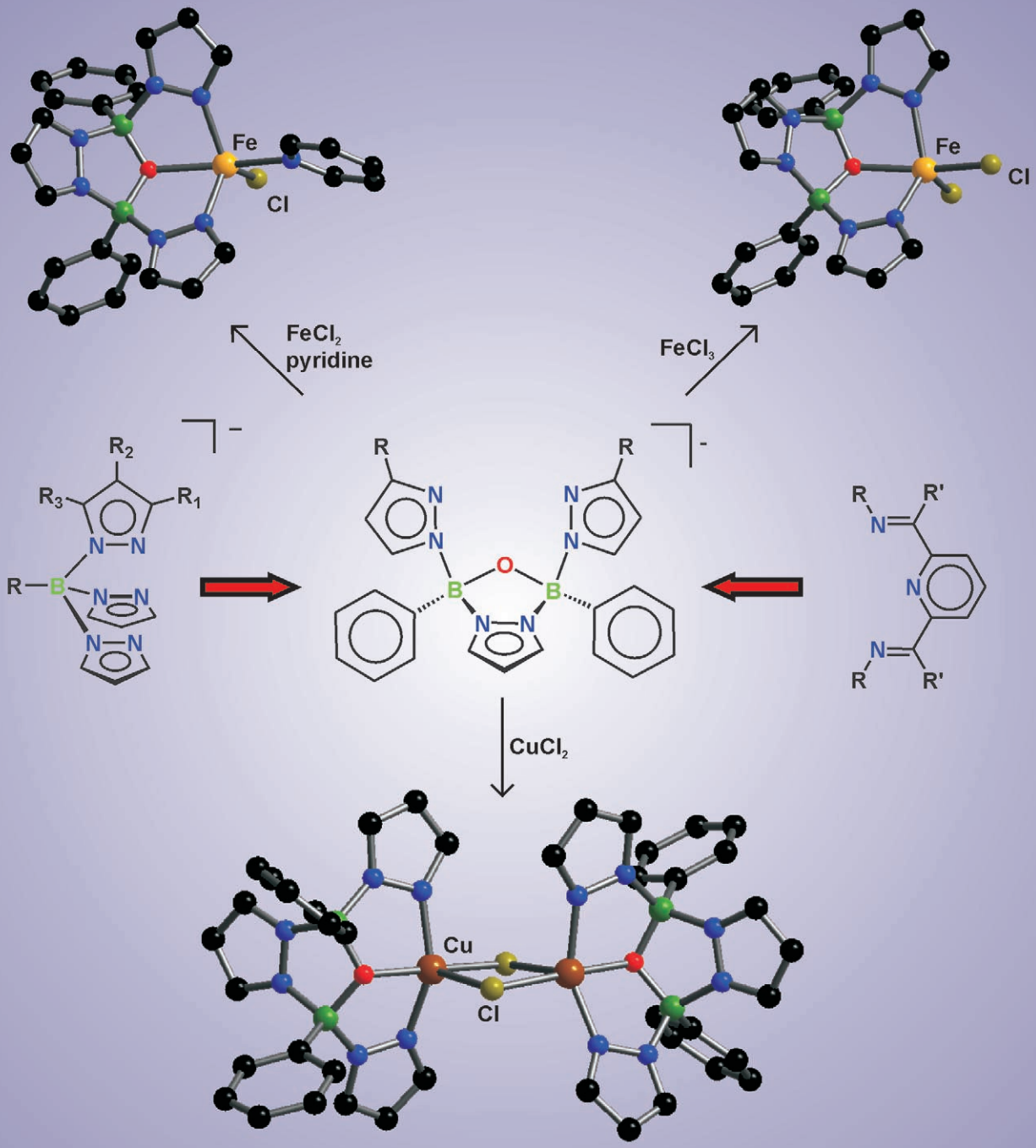

For more information see the following pages

CHEMISTRY
A EUROPEAN JOURNAL

DOI: 10.1002/chem.200600142

Modular Approach to Tridentate N,O,N′ Ligands Using Pyrazolylborate Chemistry

Susanne Bieller, Michael Bolte, Hans-Wolfram Lerner, and Matthias Wagner*[a]

Abstract: Two anionic tridentate N,O,N′ chelators, [pz(Ph)B(μ-pz)(μ-O)B(Ph)pz]$^-$ (**3**$^-$) and [pz^{Ph}(Ph)B(μ-pz)(μ-O)B(Ph)pz^{Ph}]$^-$ (**4**$^-$), as well as the corresponding complexes [Fe(**3**)(py)Cl], [Fe(**3**)Cl$_2$] and [Cu(**3**)Cl], have been synthesised and structurally characterised by X-ray crystallography (pz: pyrazolyl, pz^{Ph}: 3-phenylpyrazolyl, py: pyridine). Since our synthesis approach takes advantage of the highly modular pyrazolylborate chemistry, inexpensive and relatively resistant N,O,N′ ligands of varying steric demand are readily accessible. The complexes [Fe(**3**)(py)Cl] and [Fe(**3**)Cl$_2$] possess a distorted trigonal-bipyramidal configuration with the pyrazolyl rings occupying equatorial positions and the oxygen donor being located at an apical position. The complex [Cu(**3**)Cl] crystallises as chloro-bridged dimers featuring Cu^{II} ions with ligand environments that are intermediate between a square-planar and a trigonal-bipyramidal geometry.

Keywords: boron · chelates · ligand design · N,O ligands · pyrazolylborates

Introduction

In the field of homogeneous catalysis, tridentate ligands are widely used in order to create tailor-made molecular environments for the catalytically active metal ion and thereby to influence the (stereo)selectivity of the catalysed reaction in the desired way. Two fundamentally different classes of tridentate chelators have to be distinguished: *trans*- and *cis*-coordinating ligands. Among the former, pincer-type molecules **A**,[1–3] 2,6-bis(imino)pyridines **B**,[4–8] as well as chiral pyridine-2,6-bis(oxazoline) ligands (Pybox, **C**)[9] turned out to provide versatile platforms for the generation of many and diverse derivatives that can be specifically designed for numerous catalytic applications (Figure 1). The development of *cis*-coordinating ligands was greatly advanced by the discovery of poly(pyrazol-1-yl)borate ("scorpionate") donors **D**[10,11] 40 years ago (Figure 1). Since then, scorpionate ligands have enjoyed tremendous success, because they are readily accessible by means of a highly modular assembly. The scorpionate ligands allow for extensive variation of the substituents R^1–R^3, by which both the electronic and the steric properties of the ligand framework can be fine-tuned almost at will.

Given this background, it is our goal to exploit the advantages of pyrazolylborate chemistry also for the preparation

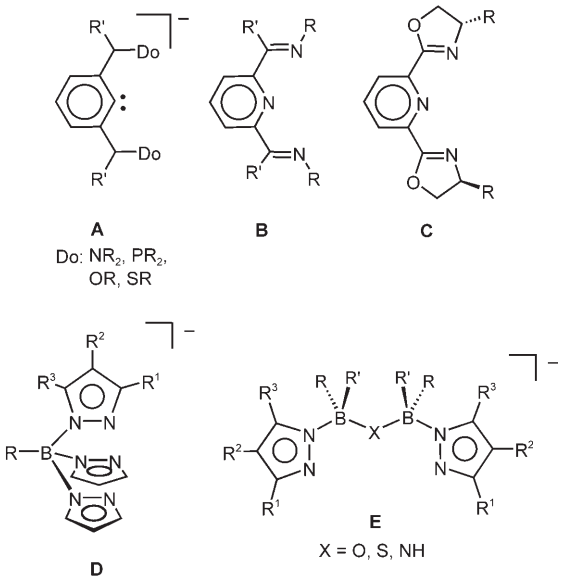

Figure 1. Tridentate meridionally coordinating pincer (**A**), 2,6-bis-(imino)pyridine (**B**), and pyridine-2,6-bis(oxazoline) (**C**) ligands; tridentate facially coordinating tris(pyrazol-1-yl)borate ligands (**D**; substituents R^1–R^3 on two pyrazolyl rings not shown); proposed tridentate meridionally coordinating bis(pyrazol-1-yl)borate ligands (**E**).

[a] S. Bieller, Dr. M. Bolte, Dr. H.-W. Lerner, Prof. Dr. M. Wagner
Institut für Anorganische Chemie
Johann Wolfgang Goethe-Universität Frankfurt am Main
Max-von-Laue-Strasse 7, 60438 Frankfurt (Germany)
Fax: (+49) 69-798-29260
E-mail: matthias.wagner@chemie.uni-frankfurt.de

of molecules with the potential to be *trans*-chelating ligands. We have selected compounds of the general structure **E** (Figure 1) as promising target molecules for which many of the established design principles in scorpionate chemistry are expected to be still valid. Appropriate choice of substituents R^1 thus offers the possibility to adjust the steric demand of **E**, whereas substituents R^2 can be employed to influence its electronic properties. To meet the specific requirements of the coordinated complex fragment, the system may further be optimised by varying the central donor site X (e.g., X = O, S, NH).

Results and Discussion

To restrict the conformational flexibility of the ligand backbone, we decided to introduce a rigid pyrazolide bridge between the two boron atoms of **E** as a substitute for two dangling R side chains. Moreover, an oxygen atom was chosen as third donor X to make the ligand as resistant as possible to hydrolysis. These considerations led to the selection of the monoanionic compound $\mathbf{3}^-$ (Scheme 1) as promising initial system for the development of *trans*-chelating scorpionate analogues.

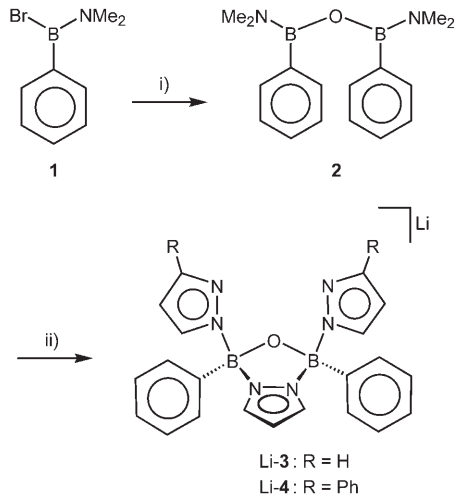

Scheme 1. Synthesis of the tridentate N,O,N′ ligands Li-**3** and Li-**4**. i) H_2O (0.5 equiv), NEt_3 (1 equiv); toluene, RT; ii) 1. Lipz (1 equiv), 2. Hpz^R (2 equiv); toluene/THF, reflux temperature.

Syntheses: The already known 1,3-diboroxane **2**[12] turned out to be a proper starting material for the preparation of $\mathbf{3}^-$ (Scheme 1). Following the published procedure,[12] **2** can be obtained in 54% yield from the reaction of *B*,*B*′,*B*″-triphenylboroxin, [-B(Ph)O-]$_3$, and bis(dimethylamino)phenylborane, $PhB(NMe_2)_2$. However, we preferred to synthesise **2** by hydrolysis of bromo(dimethylamino)phenylborane, $PhB(Br)NMe_2$,[13,14] with 0.5 equivalents of water in the presence of triethylamine (yield: 82%, cf. Experimental Section). Treatment of **2** with 1 equivalent of lithium pyrazolide (Lipz) and 2 equivalents of pyrazole (Hpz) in a toluene/THF mixture at reflux temperature leads to the clean assembly of ligand $\mathbf{3}^-$ through a transamination reaction. In contrast, according to a study conducted by Niedenzu et al.,[12] **2** reacts with 2 equivalents of Hpz in the absence of Lipz to form the bridged pyrazabole $PhB(\mu\text{-}pz)_2[\mu\text{-}OB(Ph)O]BPh$ as the major product besides substantial quantities of the 1,3-diboroxane derivative $[pz(Ph)B(\mu\text{-}pz)_2B(Ph)]_2O$. In the latter compound, two pyrazabole moieties are linked by an oxygen atom. NMR spectroscopy on the crude product $\mathbf{3}^-$ excludes the formation of *cis*-/*trans*-isomers in which the two pyrazolyl substituents would be located either at the same side or at opposite sides of the $[B(\mu\text{-}pz)(\mu\text{-}O)]$ plane. Our current working hypothesis is that the observed *cis*-selectivity of the reaction (cf. X-ray crystallography) may be due to a template effect of the Li^+ counterion. To prove the versatility of our synthesis approach, we have next prepared ligand $\mathbf{4}^-$ bearing phenyl substituents at the 3-positions of its terminal pyrazolyl groups. First, 1 equivalent of Lipz was added to **2** in toluene/THF, the mixture was then refluxed for 8 h to form the likely intermediate $Li[Me_2N(Ph)B(\mu\text{-}pz)(\mu\text{-}O)B(Ph)NMe_2]$, which was subsequently treated with 2 equivalents of Hpz^{Ph} to give $\mathbf{4}^-$ in decent yield (Scheme 1, R = Ph). The successful synthesis of $\mathbf{4}^-$ is important for perspective applications of our ligand system in homogeneous catalysis, because steric protection of the active site is often a decisive factor in catalyst design. For example, Brookhart[4] and Gibson[5] have shown that the performance as ethylene polymerisation catalysts of 2,6-bis(imino)pyridine-based Fe^{II} and Co^{II} complexes crucially depends on the presence of bulky aryl substituents R at the imino nitrogen atoms (cf. **B**, Figure 1). The Fe^{II}, Fe^{III} and Cu^{II} complexes of ligand Li-**3** are readily accessible from THF upon addition of anhydrous $FeCl_2$, $FeCl_3$ and $CuCl_2$, respectively (cf. **5**–**7**, respectively; Scheme 2). In the case of the Fe^{II} complex **5**, it was necessary to add a small amount of pyridine to obtain a well-defined single-crystalline product.

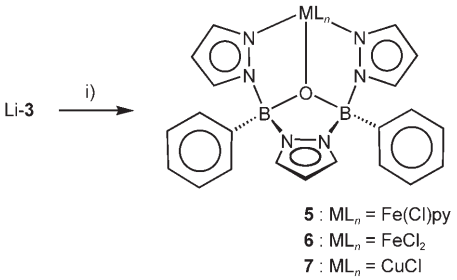

Scheme 2. Synthesis of the metal complexes **5**–**7**. i) **5**: $FeCl_2$ (1 equiv); THF/pyridine, RT; **6**: $FeCl_3$ (1 equiv); THF, RT; **7**: $CuCl_2$ (1 equiv); THF, RT.

NMR spectroscopy: The ^{11}B NMR spectra of ligands Li-**3** and Li-**4** are characterised by one single resonance at δ = 5.4 ppm testifying[15,16] to the presence of four-coordinate

boron nuclei. In its ^{1}H NMR spectrum, Li-**3** gives rise to two sets of pyrazolyl signals at $\delta = 6.27$, 7.55, 7.59 ppm (intensity ratio 2:2:2) and $\delta = 6.58$, 7.86 ppm (intensity ratio 1:2). These data are in accord with a molecular framework containing one symmetrically coordinated and two magnetically equivalent but unsymmetrically coordinated pyrazolyl rings. This interpretation is further supported by the ^{13}C NMR spectrum of Li-**3**. However, it is difficult to decide at this stage whether Li-**3** possesses *cis*- or *trans* configuration. As to be expected, the NMR parameters of Li-**3** and Li-**4** are similar, but for the fact that Li-**4** shows only two resonances for the terminal pyrazolyl fragments and that a second set of phenyl resonances can clearly be identified both in the ^{1}H and ^{13}C NMR spectra. As a result of their paramagnetic nature, meaningful NMR spectra of the complexes **5**–**7** could not be acquired.

X-ray crystallography: All the compounds under investigation were structurally characterised by X-ray crystallography. Selected crystal data and structure refinement details are compiled in Table 1. The lithium salt Li-**3** crystallises from THF/hexane with one THF molecule coordinated to the Li^+ ion (Li(thf)-**3**, triclinic space group $P\bar{1}$; Figure 2). The X-ray crystal structure analysis of Li(thf)-**3** confirms the proposed structure of the ligand framework, with one bridging and two terminal pyrazolyl groups. Most importantly, the structure analysis also shows that the latter are located in a mutual *cis*-arrangement thereby enabling $\mathbf{3}^-$ to coordinate the Li^+ ion in a tridentate fashion through two nitrogen atoms and one oxygen donor. The ligand sphere of the Li^+ centre is distorted from a tetrahedral geometry in the direction of a square-planar environment with the N-Li1-O1 bond angles being contracted to about 90° while the N12-Li1-N22 and the O1-Li1-O61 angles are expanded to 115.9(2)° and 123.8(2)°, respectively. The dihedral angle between the two pyrazolyl rings amounts to 109.7°. Despite of the supporting chelate effect and the electrostatic attraction, the Li–O contact to $\mathbf{3}^-$ is 0.052 Å longer than the bond to

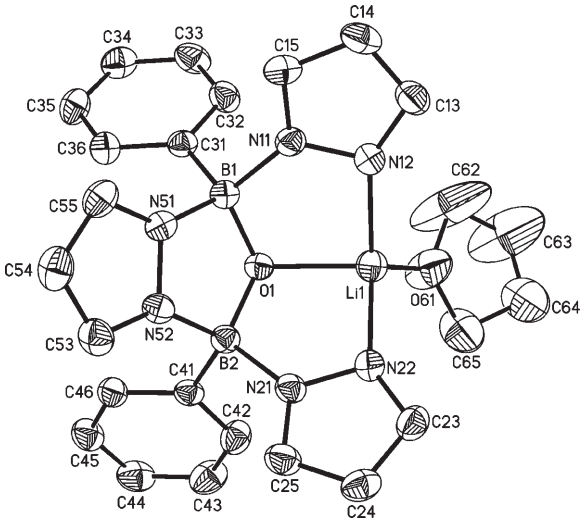

Figure 2. ORTEP plot (50% probability ellipsoids) of Li(thf)-**3**; H atoms omitted for clarity. Selected bond lengths [Å], bond angles [°] and torsion angles [°]: Li1–N12 2.023(4), Li1–N22 2.034(4), Li1–O1 1.940(4), Li1–O61 1.888(4), B1–N11 1.566(3), B1–N51 1.585(3), B1–O1 1.448(2), B2–N21 1.573(3), B2–N52 1.584(3), B2–O1 1.445(2); N12-Li1-N22 115.9(2), N12-Li1-O1 88.8(2), N22-Li1-O1 88.3(2), O1-Li1-O61 123.8(2), B1-O1-B2 115.9(2), N51-B1-O1 101.7(2), N52-B2-O1 101.6(2), O1-B1-C31 116.1(2), O1-B2-C41 116.6(2); O1-B1-N11-N12 15.5(2), O1-B2-N21-N22 −11.4(2), B1-N11-N12-Li1 −11.6(2), B2-N21-N22-Li1 1.6(2).

Table 1. Crystal data and structure refinement details for Li(thf)-**3**, Li(thf)-**4**, **5**, **6** and [(**7**)$_2$].

	Li(thf)-**3**	Li(thf)-**4**	**5**	**6**	[(**7**)$_2$]
formula	$C_{25}H_{27}B_2LiN_6O_2$	$C_{37}H_{35}B_2LiN_6O_2 \cdot 0.5\,C_6H_{14}$	$C_{26}H_{24}B_2ClFeN_7O \cdot C_4H_8O$	$C_{21}H_{19}B_2Cl_2FeN_6O$	$C_{42}H_{38}B_4Cl_2Cu_2N_{12}O_2$
M_r	472.09	667.36	635.55	519.79	984.06
colour, shape	colourless, block	colourless, block	colourless, block	dark yellow, block	blue, needle
T [K]	173(2)	173(2)	173(2)	173(2)	173(2)
crystal system	triclinic	triclinic	monoclinic	monoclinic	monoclinic
space group	$P\bar{1}$	$P\bar{1}$	$P2_1$	$P2_1/c$	$P2_1/c$
a [Å]	9.5835(10)	9.8802(5)	10.5983(9)	8.9100(4)	17.1292(13)
b [Å]	9.8411(10)	14.1338(7)	8.9755(4)	14.0959(4)	16.2248(10)
c [Å]	14.4380(15)	14.3611(7)	16.6678(12)	18.8314(9)	17.1173(13)
α [°]	74.836(8)	78.950(4)	90	90	90
β [°]	75.329(8)	72.460(4)	101.508(6)	96.752(4)	110.275(6)
γ [°]	74.406(8)	76.886(4)	90	90	90
V [Å^3]	1241.1(2)	1845.86(16)	1553.65(19)	2348.72(17)	4462.4(6)
Z	2	2	2	4	4
ρ_{calcd} [g cm^{-3}]	1.263	1.201	1.359	1.470	1.465
$F(000)$	496	706	660	1060	2008
μ [mm^{-1}]	0.081	0.074	0.611	0.896	1.125
crystal size [mm]	0.52×0.48×0.46	0.39×0.32×0.25	0.17×0.15×0.11	0.27×0.24×0.22	0.26×0.07×0.05
reflns collected	22472	50552	19796	50938	58911
independent reflns (R_{int})	4647 (0.0511)	8113 (0.0326)	5754 (0.0831)	4411 (0.0376)	8404 (0.1740)
data/restraints/parameters	4647/0/325	8113/0/461	5754/1/388	4411/0/298	8404/6/577
GOOF on F^2	1.079	1.059	1.041	1.057	1.170
$R1/wR2$ [$I > 2\sigma(I)$]	0.0555/0.1505	0.0531/0.1427	0.0533/0.0904	0.0274/0.0653	0.1347/0.3070
$R1/wR2$ (all data)	0.0674/0.1571	0.0558/0.1450	0.0691/0.0950	0.0307/0.0667	0.1662/0.3219
largest diff. peak/hole [e Å^{-3}]	0.618/−0.641	0.418/−0.354	0.246/−0.385	0.320/−0.344	3.254/−2.019

the THF ligand (Li1–O1 = 1.940(4) Å, Li1–O61 = 1.888(4) Å). The B–N bond lengths lie in the usually observed range for pyrazaboles and poly(pyrazol-1-yl)borates.[17] The B–O bonds are also unexceptional. Most of the corresponding bond angles are close to the ideal value of 109° expected for sp^3-hybridised boron atoms. The largest deviations are found for the two O-B-C angles (mean values: 116.4°) and the (μ-pz)N-B-O angles, which, as a result of their incorporation into the five-membered ring, are rather acute (N51-B1-O1 = 101.7(2)°, N52-B2-O1 = 101.6(2)°). X-ray crystallography on Li-**4**, which crystallises as a THF adduct Li(thf)-**4** (triclinic space group $P\bar{1}$; Figure 3), provides conclusive evidence that the unsubstituted pyrazolyl ring indeed occupies the B,B′-bridging position, while the 3-phenylpyrazolyl moieties act as the dangling substituents. Evidently, no pyrazolyl scrambling has occurred during ligand synthesis. As desired, the terminal pyrazolyl donors are again found in a mutual *cis*-arrangement (dihedral angle: 110.1°). The key structural parameters of Li(thf)-**4** are essentially the same as in the case of Li(thf)-**3**, with the notable exception that the Li1–O61 bond in Li(thf)-**4** is elongated by 0.032 Å to a value of 1.920(2) Å. This finding indicates that, similar to the chemistry of poly(pyrazol-1-yl)borate ligands, attachment of bulky phenyl substituents to the terminal pyrazolyl rings leads to a measurable steric shielding of the coordinated metal ion.

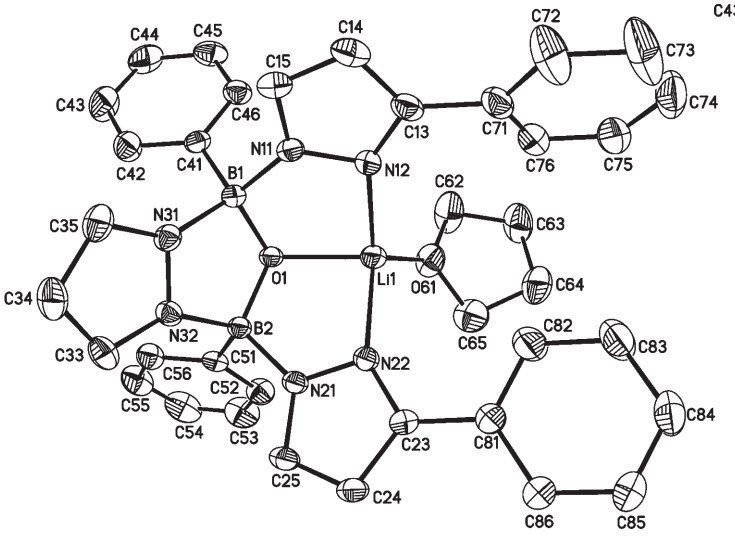

Figure 3. ORTEP plot (50% probability ellipsoids) of Li(thf)-**4**; H atoms omitted for clarity. Selected bond lengths [Å], bond angles [°] and torsion angles [°]: Li1–N12 2.035(3), Li1–N22 2.051(2), Li1–O1 1.942(2), Li1–O61 1.920(2), B1–N11 1.578(2), B1–N31 1.592(2), B1–O1 1.455(2), B2–N21 1.579(2), B2–N32 1.587(2), B2–O1 1.458(2); N12-Li1-N22 114.9(1), N12-Li1-O1 90.1(1), N22-Li1-O1 88.7(1), O1-Li1-O61 122.3(1), B1-O1-B2 115.8(1); O1-B1-N11-N12 14.7(2), O1-B2-N21-N22 −1.7(2), B1-N11-N12-Li1 −13.5(1), B2-N21-N22-Li1 −10.0(1).

The Fe^{II} complex **5** (monoclinic, $P2_1$; Figure 4) contains a five-coordinate iron centre that binds to a chloro ligand, a pyridine molecule and the tridentate chelator $\mathbf{3}^-$. For five-

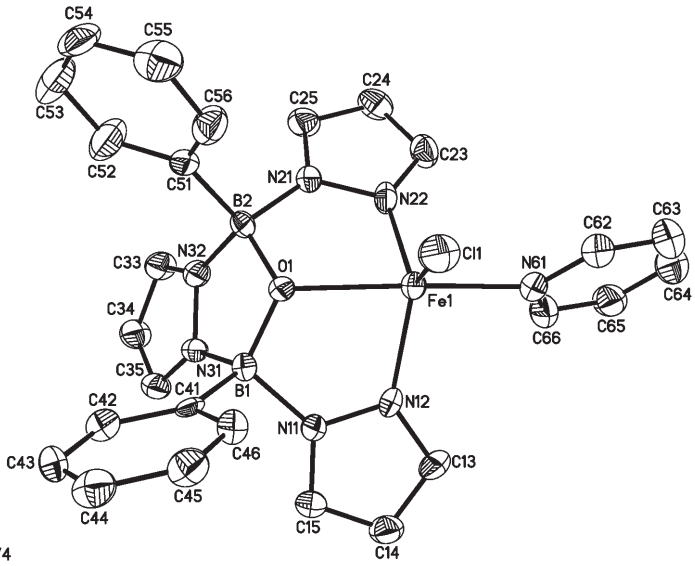

Figure 4. ORTEP plot (50% probability ellipsoids) of **5**; H atoms omitted for clarity. Selected bond lengths [Å], bond angles [°] and torsion angles [°]: Fe1–N12 2.082(3), Fe1–N22 2.084(4), Fe1–N61 2.180(4), Fe1–O1 2.179(3), Fe1–Cl1 2.292(1); N12-Fe1-N22 117.9(2), N12-Fe1-N61 93.7(1), N12-Fe1-O1 78.4(1), N12-Fe1-Cl1 119.7(1), N22-Fe1-N61 89.3(1), N22-Fe1-O1 78.5(1), N22-Fe1-Cl1 120.4(1), N61-Fe1-O1 159.9(1), N61-Fe1-Cl1 101.1(1), O1-Fe1-Cl1 98.9(1); O1-B1-N11-N12 5.7(5), O1-B2-N21-N22 −3.7(5), B1-N11-N12-Fe(1) 2.8(5), B2-N21-N22-Fe1 −3.7(4).

coordinate complexes, the parameter $\tau = (\theta - \phi)/60°$[18] provides a quantitative measure of whether the ligand sphere more closely approaches a square-pyramidal ($\tau = 0$) or a trigonal-bipyramidal geometry ($\tau = 1$; θ, ϕ are the two largest bond angles and $\theta > \phi$). In the case of **5**, we have θ = N61-Fe1-O1 = 159.9(1)° and ϕ = N22-Fe1-Cl1 = 120.4(1)°, such that τ possesses a value of 0.66. The coordination geometry about the Fe^{II} ion is thus best described as distorted trigonal bipyramidal with the pyridine molecule and the oxygen atom occupying the apical positions. All angles between equatorial ligands are close to 120° (N12-Fe1-N22 = 117.9(2)°, N12-Fe1-Cl1 = 119.7(1)°, N22-Fe1-Cl1 = 120.4(1)°). The two pyrazolyl rings include a dihedral angle of 129.4°. As to be expected for geometric and electrostatic reasons, the mean Fe–N(pz) bond length is smaller by 0.097 Å than the Fe1–N61 = 2.180(4) Å contact. Accordingly, the Fe–N(pz) bonds of **5** are also shorter than those of the related complex $[Fe(L)Cl_2]$[19] bearing a neutral ligand L = 2,6-bis(3,5-dimethyl-*N*-pyrazolyl)pyridine (**5**: mean value = 2.083 Å; $[Fe(L)Cl_2]$: mean value = 2.158 Å). The Fe–Cl bond lengths in **5** (Fe1–Cl1 = 2.292(1) Å) and $[Fe(L)Cl_2]$ (Fe–Cl = 2.304(2), 2.308(1) Å), however, are almost identical within experimental error. Complex **5** crystallises together with 1 equivalent of THF, the oxygen atom of which forms a short contact to one of the pyridine *ortho*-H atoms ((THF)O···H(pyridine) = 2.662 Å).

A similar ligand arrangement as in **5** is observed in the Fe^{III} complex **6** (monoclinic space group $P2_1/c$; Figure 5), apart from the fact that a chloro ligand is substituted for the pyridine donor in the apical position (O1-Fe1-Cl2 =

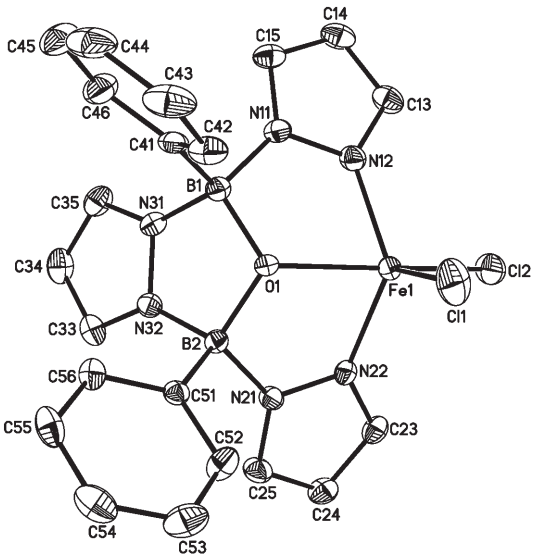

Figure 5. ORTEP plot (50% probability ellipsoids) of **6**; H atoms omitted for clarity. Selected bond lengths [Å], bond angles [°] and torsion angles [°]: Fe1–N12 2.027(1), Fe1–N22 2.030(1), Fe1–O1 2.119(1), Fe1–Cl1 2.219(1), Fe1–Cl2 2.239(1); N12-Fe1-N22 125.2(1), N12-Fe1-O1 78.5(1), N12-Fe1-Cl1 118.2(1), N12-Fe1-Cl2 93.3(1), N22-Fe1-O1 78.9(1), N22-Fe1-Cl1 112.8(1), N22-Fe1-Cl2 93.1(1), O1-Fe1-Cl1 94.5(1), O1-Fe1-Cl2 161.8(1), Cl1-Fe1-Cl(2) 103.7(1); O1-B1-N11-N12 2.7(2), O1-B2-N21-N22 −0.4(2), B1-N11-N12-Fe1 −5.2(2), B2-N21-N22-Fe1 7.8(2).

161.8(1)°) and that the N12-Fe1-N22 angle is expanded to 125.2(1)° as compared to only 117.9(2)° in **5** (**6**: $\tau = 0.61$; dihedral angle between the pyrazolyl rings = 139.8°). Due to the trivalent oxidation state of the central iron atom, all Fe–X bond lengths are shorter in **6** than the corresponding bond lengths in **5** (X = N, O, Cl).

The Cu^{II} complex **7** crystallises in the monoclinic space group $P2_1/c$ and forms chloro-bridged dimers $[(\mathbf{7})_2]$ in the solid state (Figure 6). The individual monomeric units possess pronouncedly planarised structures with bond angles N12-Cu1-N22 = 150.2(4)° and N62-Cu2-N72 = 147.4(4)°. The corresponding dihedral angles between the pyrazolyl rings are 153.3° and 140.6°. Most importantly, both halves of the dimer molecule have a τ value of 0.46 indicating the ligand environment of each Cu^{II} ion in $[(\mathbf{7})_2]$ to be closer to a square-pyramidal rather than a trigonal bipyramidal configuration. Steel et al. have recently published a Cu^{II} complex $[Cu(L')Cl_2]$ (L′ = 8-(2-pyridylmethoxy)quinoline) that bears a tridentate N,O,N′ ligand with sp^2-hybridised nitrogen atoms and, moreover, establishes a distorted square-pyramidal geometry in the crystal lattice ($\tau = 0.27$).[20] A comparison of $[(\mathbf{7})_2]$ with $[Cu(L')Cl_2]$ reveals somewhat shorter Cu–N bond lengths in the former (mean value = 1.962 Å) than in the latter compound (mean value = 1.992 Å). Differences in $Cu–Cl_{eq}$ bond lengths are small between both compounds ($[(\mathbf{7})_2]$: Cu1–Cl2 = 2.294(3) Å, Cu2–Cl1 = 2.292(3) Å; $[Cu(L')Cl_2]$: $Cu–Cl_{eq}$ = 2.244(1) Å), whereas a large discrepancy is observed for the Cu–O contacts ($[(\mathbf{7})_2]$: Cu1–O1 = 2.035(8) Å, Cu2–O2 = 2.015(7) Å; $[Cu(L')Cl_2]$: Cu–O = 2.170(1) Å). As an explanation, one has again to bear in mind that $[(\mathbf{7})_2]$ contains anionic ligands, whereas L′ is uncharged. Moreover, the oxygen atoms of $[(\mathbf{7})_2]$ are bonded to two electropositive four-coordinate boron atoms; this probably leads to a pronounced accumulation of negative partial charge and in turn to a contraction of the Cu–O bond.

Conclusion

Tris(pyrazol-1-yl)borate ("scorpionate") ligands are a well-established class of *cis*-coordinating tridentate chelators. Their highly modular assembly makes a multitude of differ-

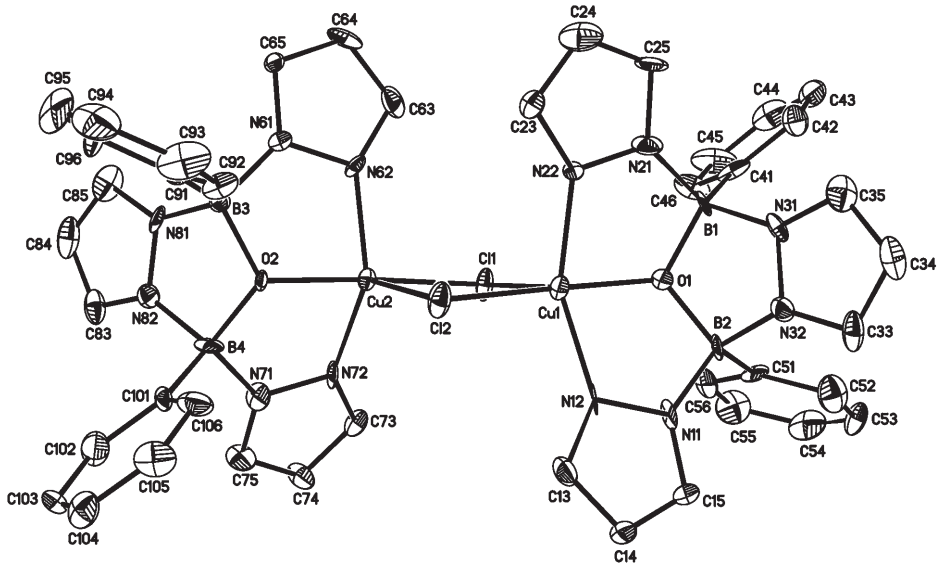

Figure 6. ORTEP plot (50% probability ellipsoids) of $[(\mathbf{7})_2]$; H atoms omitted for clarity. Selected bond lengths [Å], atom···atom distances [Å], bond angles [°] and torsion angles [°]: Cu1–N12 1.960(11), Cu1–N22 1.977(9), Cu1–O1 2.035(8), Cu1–Cl1 2.637(3), Cu1–Cl2 2.294(3), Cu2–N62 1.972(10), Cu2–N72 1.940(11), Cu2–O2 2.015(7), Cu2–Cl1 2.292(3), Cu2–Cl2 2.767(4), Cu1···Cu2 3.545(2); N12-Cu1-N22 150.2(4), N12-Cu1-O1 83.3(3), N22-Cu1-O1 84.4(4), N12-Cu1-Cl1 107.7(3), N12-Cu1-Cl2 95.3(3), N22-Cu1-Cl1 99.6(3), N22-Cu1-Cl2 96.1(3), O1-Cu1-Cl1 90.8(2), O1-Cu1-Cl2 177.8(3), N62-Cu2-N72 147.4(4), N62-Cu2-O2 84.6(4), N72-Cu2-O2 83.8(4), N62-Cu2-Cl1 98.3(3), N62-Cu2-Cl2 97.9(3), N72-Cu2-Cl1 95.6(3), N72-Cu2-Cl2 112.0(3), O2-Cu2-Cl1 175.0(3), O2-Cu2-Cl2 87.6(2), Cl1-Cu1-Cl2 91.2(1), Cl1-Cu2-Cl2 88.0(1), Cu1-Cl1-Cu2 91.7(1), Cu1-Cl2-Cu2 88.4(1); O1-B1-N21-N22 3.1(15), O1-B2-N11-N12 −11.1(15), O2-B3-N61-N62 0.3(14), O2-B4-N71-N72 −1.1(15), B1-N21-N22-Cu1 4.6(14), B2-N11-N12-Cu1 2.8(14), B3-N61-N62-Cu2 7.7(13), B4-N71-N72-Cu2 −3.2(13).

ent tailor-made derivatives readily available. It is our aim to exploit the advantages of pyrazolylborate chemistry for the development of N,O,N′ tridentate and *trans*-chelating ligands. To this end, we prepared two anionic tridentate N,O,N′ ligands, $[pz(Ph)B(\mu\text{-}pz)(\mu\text{-}O)B(Ph)pz]^-$ (**3**$^-$) and $[pz^{Ph}(Ph)B(\mu\text{-}pz)(\mu\text{-}O)B(Ph)pz^{Ph}]^-$ (**4**$^-$), and investigated their coordination behaviour towards Fe^{II}, Fe^{III} and Cu^{II} centres. Depending from the nature of the coordinated complex fragment, **3**$^-$ turned out to achieve (pz)N-M-N(pz) bite angles between 117.9(2)° and 150.2(4)° (pz: pyrazolyl; pz^{Ph}: 3-phenylpyrazolyl). In contrast, the corresponding bite angles in tris(pyrazol-1-yl)borate complexes of iron and copper are found within an interval of 80°–104°[17] and 80°–103°,[17] respectively (no restrictions to oxidation state and coordination number of the metal centres were applied). A further flattening of the ligand framework of **3**$^-$ is most likely to be incompatible with the simultaneous presence of 1) an sp^3 oxygen donor, 2) sp^3 boron atoms and 3) the pyrazolyl brace (cf. Figure 7). Comparable and truly *trans*-coordinating ligands are either conformationally more flexible (e.g., $[(ArNCH_2CH_2)_2O]^{2-}$; Ar = 2,6-$Me_2C_6H_3$, 2,6-$iPr_2C_6H_3$)[21] or feature exclusively sp^2-hybridised atoms along the ligand backbone (e.g., 4,6-dibenzofurandiyl-2,2′-bis(4-phenyloxazoline)[22] and 2,6-bis(pyrazol-1-yl)pyridine[19,23]). Interestingly, the $[(t\text{BuN-}o\text{-}C_6H_4)_2O]^{2-}$ ligand, which is an analogue of $[(ArNCH_2CH_2)_2O]^{2-}$ with a more rigid backbone, was found to adopt a coordination mode similar to **3**$^-$ rather than to $[(ArNCH_2CH_2)_2O]^{2-}$.[24] In summary, ligands **3**$^-$ and **4**$^-$ represent the first pincer-type N,O,N′ ligands that are based on pyrazolylborate chemistry. They are easy to derivatise and exhibit a flexible coordination mode that makes them useful in many areas of coordination chemistry.

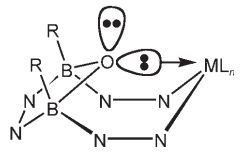

Figure 7. Structural peculiarities of ligand **3**$^-$ preventing a fully planar tridentate coordination mode.

Experimental Section

General considerations: All reactions and manipulations of air-sensitive compounds were carried out in dry, oxygen-free nitrogen using standard Schlenk glassware. Solvents were freshly distilled under argon from Na/benzophenone (toluene, THF), Na/Pb alloy (hexane, heptane) or stored over 4 Å molecular sieves prior to use (CH_2Cl_2, CD_3CN). NMR: Bruker Avance 400, Bruker AM 250, Bruker DPX 250 spectrometers. ^{11}B NMR spectra are reported relative to external $BF_3{\cdot}Et_2O$. Unless stated otherwise, all NMR spectra were run at ambient temperature. Abbreviations: s = singlet; d = doublet; t = triplet; vt = virtual triplet; dd = doublet of doublets; br = broad; n.r. = multiplet expected in the ^1H NMR spectrum but not resolved; n.o. = signal not observed; Me = methyl; Ph = phenyl; py = pyridine, pz = pyrazolide, THF = tetrahydrofuran. Elemental analyses were performed by the microanalytical laboratory of the University of Frankfurt and by Quantitative Technologies Inc. (QTI). Compound **1** can be synthesised according to a literature procedure.[13]

Synthesis of 2: Water (63 μL, 0.063 g, 3.50 mmol) and triethylamine (0.713 g, 7.05 mmol) were added to a solution of **1** (1.484 g, 7.00 mmol) in toluene (20 mL) at RT with stirring whereupon a colourless precipitate formed. The resulting slurry was stirred for 8 h, the precipitate collected on a frit (G4) and the filtrate evaporated in vacuo. The off-white, slightly oily product obtained can be used without further purification. Yield: 0.802 g (2.86 mmol, 82 %); ^{11}B NMR (128.4 MHz, $CDCl_3$): $\delta = 29.8$ ppm ($h_{1/2} = 270$ Hz); ^1H NMR (250.1 MHz, $CDCl_3$): $\delta = 2.60$, 2.72 (2 s, 2 × 6 H; CH_3), 7.08–7.14 ppm (m, 10 H; PhH); ^{13}C NMR (62.9 MHz, $CDCl_3$): $\delta =$ 36.4, 38.8 (CH_3), 127.1 (PhC_p), 127.4 (PhC_m), 132.5 ppm (PhC_o), n.o. (C–B).

Synthesis of Li(thf)-3: Lithium pyrazolide (0.847 g, 11.45 mmol) and pyrazole (1.556 g, 22.86 mmol) in THF (10 mL) were added to a solution of **2** (3.199 g, 11.43 mmol) in toluene (20 mL) with stirring. The resulting solution was heated to reflux temperature for 8 h, the solvent was removed in vacuo and the resulting colourless solid residue washed with hexane (10 mL). X-ray quality crystals of Li(thf)-**3** were grown by layering a solution of the crude product in THF with hexane. Yield of Li(thf)-**3**: 3.443 g (7.29 mmol, 64 %); ^{11}B NMR (128.4 MHz, CD_3CN): $\delta =$ 5.4 ppm ($h_{1/2} = 160$ Hz); ^1H NMR (400.1 MHz, CD_3CN): $\delta = 6.27$ (vt, ^3J(H,H) = 1.9 Hz, 2 H; pzH-4), 6.58 (t, ^3J(H,H) = 2.2 Hz, 1 H; μ-pzH-4), 7.08–7.11 (m, 6 H; PhH_m, PhH_p), 7.14–7.17 (m, 4 H; PhH_o), 7.55 (d, ^3J(H,H) = 1.7 Hz, 2 H; pzH-3 or 5), 7.59 (d, ^3J(H,H) = 2.2 Hz, 2 H; pzH-5 or 3), 7.86 ppm (d, ^3J(H,H) = 2.2 Hz, 2 H; μ-pzH-3,5); ^{13}C NMR (100.6 MHz, CD_3CN): $\delta = 106.4$ (pzC-4), 110.8 (μ-pzC-4), 127.4 (PhC_p), 127.9 (PhC_m), 131.1 (μ-pzC-3,5), 132.5 (PhC_o), 132.9 (pzC-5 or 3), 139.1 ppm (pzC-3 or 5), n.o. (C–B); elemental analysis calcd (%) for $C_{21}H_{19}B_2LiN_6O{\cdot}C_4H_8O{\cdot}0.5\,H_2O$ (481.10): C 62.41, H 5.87, N 17.46; found: C 62.19, H 5.67, N 17.25.

Synthesis of Li(thf)-4: Neat lithium pyrazolide (0.225 g, 3.04 mmol) was added to a solution of **2** (0.850 g, 3.04 mmol) in toluene (20 mL) and THF (5 mL) with stirring. After the resulting solution had been heated to reflux temperature for 8 h, it was allowed to cool to RT for the addition of 3-phenylpyrazole (0.877 g, 6.08 mmol). The mixture was refluxed for further 8 h, all volatiles were removed in vacuo and the resulting colourless solid residue was washed with hexane (10 mL). X-ray quality crystals of Li(thf)-**4** were grown by layering a solution of the crude product in THF with hexane. Yield of Li(thf)-**4**: 1.003 g (1.61 mmol, 53 %); ^{11}B NMR (128.4 MHz, CD_3CN): $\delta = 5.4$ ppm ($h_{1/2} = 180$ Hz); ^1H NMR (250.1 MHz, CD_3CN): $\delta = 6.61$ (d, ^3J(H,H) = 2.3 Hz, 2 H; PhpzH-4), 6.65 (t, ^3J(H,H) = 2.3 Hz, 1 H; μ-pzH-4), 7.14–7.18 (m, 6 H; PhH_m, PhH_p), 7.23–7.27 (m, 10 H; PhH_o, $PhpzH_m$, $PhpzH_p$), 7.68–7.72 (m, 4 H; $PhpzH_o$), 7.70 (d, ^3J(H,H) = 2.2 Hz, 2 H; PhpzH-5), 7.98 ppm (d, ^3J(H,H) = 2.3 Hz, 2 H; μ-pzH-3,5); ^{13}C NMR (100.6 MHz, CD_3CN): $\delta = 104.6$ (PhpzC-4), 111.3 (μ-pzC-4), 126.7 ($PhpzC_o$), 127.7 (PhC_p), 128.2 (PhC_m), 128.4 ($PhpzC_p$), 129.7 ($PhpzC_m$), 131.6 (μ-pzC-3,5), 132.5 (PhC_o), 134.7, 134.8 (PhpzC-3,5), 152.0 ppm ($PhpzC_i$), n.o. (C–B); elemental analysis calcd (%) for $C_{33}H_{27}B_2LiN_6O{\cdot}C_4H_8O{\cdot}0.5\,C_6H_{14}$ (667.36): C 71.99, H 6.34, N 12.59; found: C 71.17, H 6.24, N 12.65.

Synthesis of 5: The ligand Li(thf)-**3** (0.195 g, 0.41 mmol) was dissolved in a mixture of THF (15 mL) and pyridine (2 mL). Neat $FeCl_2$ (0.053 g, 0.41 mmol) was added at RT. After the reaction mixture had been stirred for 10 h, the resulting yellow solution was evaporated and the yellow residue recrystallised from THF/hexane (1:3). Yield of crystalline **5**: 0.123 g (0.22 mmol, 54 %); LR-MS (MALDI$^+$): *m*/*z* (%): 563 (37) $[M]^+$; elemental analysis calcd (%) for $C_{26}H_{24}B_2ClFeN_7O{\cdot}C_4H_8O$ (635.55): C 56.70, H 5.08, N 15.42; found: C 56.25, H 5.04, N 15.86.

Synthesis of 6: Neat $FeCl_3$ (0.069 g, 0.42 mmol) was added at RT to a solution of Li(thf)-**3** (0.200 g, 0.42 mmol) in THF (20 mL). After stirring for 10 h, the red solution was evaporated to dryness in vacuo. The resulting red residue was extracted into CH_2Cl_2 (10 mL). Layering of the solution of the residue in CH_2Cl_2 with hexane gave red crystals suitable for an X-ray crystal structure analysis. Yield of crystalline **6**: 0.154 g (0.30 mmol, 71 %); elemental analysis calcd (%) for $C_{21}H_{19}B_2Cl_2FeN_6O$ (519.79): C 48.52, H 3.68, N 16.16; found: C 48.46, H 3.58, N 15.96.

Synthesis of 7: Neat anhydrous $CuCl_2$ (0.042 g, 0.31 mmol) was added at RT to Li(thf)-**3** (0.145 g, 0.31 mmol) in THF (12 mL). During the first 5 min of stirring, the colour of the reaction mixture changed from blue to

green. After 10 h, the solution was evaporated and the resulting green oily residue extracted into CH_2Cl_2 (10 mL). Layering of the solution of the residue in CH_2Cl_2 with heptane gave turquoise crystals of [(**7**)$_2$] suitable for an X-ray crystal structure analysis. Yield of crystalline **7**: 0.116 g (0.24 mmol, 77 %); elemental analysis calcd (%) for $C_{21}H_{19}B_2ClCuN_6O$ (492.03): C 51.26, H 3.89, N 17.08; found: C 51.20, H 3.93, N 17.18.

Crystal structure determinations of Li(thf)-3, Li(thf)-4, 5, 6 and [(7)$_2$]: Data collections were performed on a Stoe-IPDS-II two-circle diffractometer with graphite-monochromated $Mo_{K\alpha}$ radiation ($\lambda = 0.71073$ Å). Empirical absorption corrections with the MULABS option[25] in the program PLATON[26] were performed. The structures were solved by direct methods[27] and refined with full-matrix least-squares on F^2 using the program SHELXL97.[28] Hydrogen atoms were placed on ideal positions and refined with fixed isotropic displacement parameters using a riding model. Ligand Li(thf)-**4** crystallises together with half a molecule of hexane in the asymmetric unit. The crystal lattice of **5** contains one equivalent of THF solvate molecules; for **5** the absolute structure was determined: Flack x parameter = 0.08(2). CCDC-294679 (Li(thf)-**3**), CCDC-294680 (Li(thf)-**4**), CCDC-294681 (**5**), CCDC-294682 (**6**) and CCDC-294683 ([(**7**)$_2$]) contain the supplementary crystallographic data for this paper. These data can be obtained free of charge from The Cambridge Crystallographic Data Centre via www.ccdc.cam.ac.uk/data_request/cif.

Acknowledgement

The authors are grateful to the Deutsche Forschungsgemeinschaft (DFG) and the Fonds der Chemischen Industrie (FCI) for financial support.

[1] M. Albrecht, G. van Koten, *Angew. Chem.* **2001**, *113*, 3866–3898; *Angew. Chem. Int. Ed.* **2001**, *40*, 3750–3781.
[2] M. E. van der Boom, D. Milstein, *Chem. Rev.* **2003**, *103*, 1759–1792.
[3] J. T. Singleton, *Tetrahedron* **2003**, *59*, 1837–1857.
[4] B. L. Small, M. Brookhart, A. M. A. Bennett, *J. Am. Chem. Soc.* **1998**, *120*, 4049–4050.
[5] G. J. P. Britovsek, V. C. Gibson, B. S. Kimberley, P. J. Maddox, S. J. McTavish, G. A. Solan, A. J. P. White, D. J. Williams, *Chem. Commun.* **1998**, 849–850.
[6] G. J. P. Britovsek, S. Mastroianni, G. A. Solan, S. P. D. Baugh, C. Redshaw, V. C. Gibson, A. J. P. White, D. J. Williams, M. R. J. Elsegood, *Chem. Eur. J.* **2000**, *6*, 2221–2231.
[7] S. Park, Y. Han, S. K. Kim, J. Lee, H. K. Kim, Y. Do, *J. Organomet. Chem.* **2004**, *689*, 4263–4276.
[8] G. J. P. Britovsek, J. England, S. K. Spitzmesser, A. J. P. White, D. J. Williams, *Dalton Trans.* **2005**, 945–955.
[9] G. Desimoni, G. Faita, P. Quadrelli, *Chem. Rev.* **2003**, *103*, 3119–3154.
[10] S. Trofimenko, *Chem. Rev.* **1993**, *93*, 943–980.
[11] S. Trofimenko, *Scorpionates—The Coordination Chemistry of Polypyrazolylborate Ligands*, Imperial College Press, London, **1999**.
[12] J. Bielawski, K. Niedenzu, *Inorg. Chem.* **1986**, *25*, 1771–1774.
[13] P. A. Barfield, M. F. Lappert, J. Lee, *J. Chem. Soc. A* **1968**, 554–559.
[14] C. Brown, R. H. Cragg, T. J. Miller, D. O. Smith, *J. Organomet. Chem.* **1983**, *244*, 209–215.
[15] "Nuclear Magnetic Resonance Spectroscopy of Boron Compounds": H. Nöth, B. Wrackmeyer in *NMR Basic Principles and Progress* (Eds.: P. Diehl, E. Fluck, R. Kosfeld), Springer, Berlin, **1978**.
[16] J. Mason, *Multinuclear NMR*, Plenum, New York, **1987**.
[17] F. H. Allen, *Acta Crystallogr. Sect. B* **2002**, *58*, 380–388 (Cambridge Crystallographic Database, CSD Version 5.27, November **2005**).
[18] A. W. Addison, T. N. Rao, J. Reedijk, J. van Rijn, G. C. Verschoor, *J. Chem. Soc. Dalton Trans.* **1984**, 1349–1356.
[19] F. Calderazzo, U. Englert, C. Hu, F. Marchetti, G. Pampaloni, V. Passarelli, A. Romano, R. Santi, *Inorg. Chim. Acta* **2003**, *344*, 197–206.
[20] M. R. A. Al-Mandhary, P. J. Steel, *Inorg. Chim. Acta* **2003**, *351*, 7–11.
[21] R. R. Schrock, F. Schattenmann, M. Aizenberg, W. M. Davis, *Chem. Commun.* **1998**, 199–200.
[22] S. Kanemasa, Y. Oderaotoshi, S. Sakaguchi, H. Yamamoto, J. Tanaka, E. Wada, D. P. Curran, *J. Am. Chem. Soc.* **1998**, *120*, 3074–3088.
[23] D. L. Jameson, K. A. Goldsby, *J. Org. Chem.* **1990**, *55*, 4992–4994.
[24] R. Baumann, W. M. Davis, R. R. Schrock, *J. Am. Chem. Soc.* **1997**, *119*, 3830–3831.
[25] R. H. Blessing, *Acta Crystallogr. Sect. A* **1995**, *51*, 33–38.
[26] A. L. Spek, *Acta Crystallogr. Sect. A* **1990**, *46*, C34.
[27] G. M. Sheldrick, *Acta Crystallogr. Sect. A* **1990**, *46*, 467–473.
[28] G. M. Sheldrick, SHELXL-97, A Program for the Refinement of Crystal Structures, Universität Göttingen, Göttingen, **1997**.

Received: February 2, 2006
Published online: May 19, 2006

